

# Obtaining a nanoporous Layer by the Anodizing Process on AISI 316L Steel to Obtain Better Corrosion Resistance Properties in Metallic Biomaterials Applications

M. Petry<sup>a</sup>, L.G. Soares<sup>\*a</sup> , E.L. Schneider<sup>b</sup> , A.L. Ziulkoski<sup>a</sup>,

F.D.P. Morisso<sup>a</sup>, S.R. Kunst<sup>c</sup> , C.T. Oliveira<sup>a</sup>

<sup>a</sup>Universidade FEEVALE, Laboratório de Estudos Avançados em Materiais, Vila Nova, 93352-000, Novo Hamburgo, RS, Brasil.

<sup>b</sup>Universidade Federal do Rio Grande do Sul, Departamento de Engenharia de Materiais, Av. Bento Gonçalves, 9500, Bairro Agronomia, 91501970, Porto Alegre, RS, Brasil.

<sup>c</sup>Projeto de Fixação de Recursos Humanos do CNPq – Nível A (RHAE), Sapucaia do Sul, RS, Brasil.

Received: August 15, 2023; Revised: January 19, 2024; Accepted: March 28, 2024

AISI 316L is a metallic biomaterial used in Unified Health System (SUS) due to low cost. However, corrosion in AISI 316L is a major cause of premature failure and toxic reactions to implants. Nanotubular or nanoporous anodized layers have proven to be good and affordable alternatives to create greater interaction and less damage to human tissue. Thus, the main of this study was to obtain a nanoporous layer by anodizing on AISI 316L, aiming to improve its corrosion resistance for use as a biomaterial. AISI 316L were anodized in 10M NaOH, 0.6mA/cm<sup>2</sup> for 5 and 10min. Transients of current density and potential and oxide color were evaluated. Anodized layers were characterized by scanning electron microscopy, X-ray diffraction analysis and electrochemical assays. Nanoporous anodized layers with nanoplate arrangement were obtained. The 5min anodized sample showed better corrosion resistance than the original steel, being considered promising for use as a biomaterial.

**Keywords:** AISI 316L, Stainless Steel, Anodizing; Biomaterial.

## 1. Introduction

AISI 316L austenitic stainless steel remains one of the most used materials in traumatological and orthopedic applications as implants by the Unified Health System (SUS) in Brazil, according to data from 2019<sup>1</sup>. AISI 316L is more widely available and presents lower cost than commercially pure titanium, and it meets the required properties of mechanical and corrosion resistance<sup>2</sup>. However, in contact with body fluids, corrosion resistance of AISI 316L can be compromised<sup>3</sup>.

Corrosive processes are the main causes of post-surgical complications, such as rejection, inflammation, allergic reactions and infections, often leading to the need for new surgeries and the use of additional medications<sup>4</sup>.

Furthermore, corrosion restricts its useful life to a shorter time and worsens the patient's health, demanding replacement of the material<sup>5</sup>.

Several studies point to improvements in osseointegration on surfaces of implants or prostheses with the presence of transition metal oxide nanotubes or nanopores<sup>6</sup>.

In this sense, many surface treatments have been used on 316L stainless steel in order to optimize both the surface properties and the osseointegration process thus turning it comparable to titanium. The development and use of these techniques are based on the theory that increased bone/implant contact can be achieved by changing the

topography or by increasing the surface roughness of the implant<sup>7</sup>. Treatments include processes for modifying these characteristics, such as sandblasting, acid etching, anodic oxidation, coating with a layer of biocompatible materials, ion implantation and plasma vapor deposition techniques. Some of these techniques are currently used in implants sold on the world market<sup>8</sup>. Among them, anodic oxidation is one of the most common and flexible methods used to modify metallic surfaces at a nanoscale. Anodic oxidation has been used successfully to transform metallic surfaces into nanotubular structures with diameters less than 100 nm<sup>9</sup>. In addition, by simply adjusting process parameters, such as electrolyte composition, applied current and potential density, the chemical and topographical properties of the surface can be precisely modulated, allowing for the complete control of its characteristics<sup>10</sup>. Such peculiar characteristics of the anodic oxidation make it very attractive for use on industrial scale as a surface treatment.

In the study by Kowalsk et al.<sup>9</sup>, the authors aimed to obtain a thick (greater than 1.0 μm) insoluble nanoporous oxide layer on AISI 304 for subsequent biofunctionalization. To this end, simple anodization with direct current in a sulfuric acid-based electrolyte was used. The anodized sample had a whitish gray color that did not exceed a thickness of 50 nm and is mainly composed of chromium oxide complex. The surface texture is composed of granular crystals on the order of tenths of microns. As a result, nanopores were formed, although shallow in depth.

\*e-mail: [lugoies.soares@gmail.com](mailto:lugoies.soares@gmail.com)

In a more recent study to obtain thick porous anodic oxide films, Wang et al.<sup>11</sup> carried out a series of experiments varying time and voltage with the purpose of modeling the growth mechanism and pore morphology in the anodic oxide layer of AISI 304. For this purpose, anodization was carried out with ethylene glycol electrolyte containing 0.1 M of distilled water and 0.1 M ammonium fluoride. In this study, the action of the F<sup>-</sup> ion as a promoter of the formation of pores in the oxide layer is observed. In the analysis of the chemical composition of the oxide layer by electronic X-ray spectroscopy, a predominance of Cr<sub>2</sub>O<sub>3</sub> and  $\alpha$ -Fe<sub>2</sub>O<sub>3</sub> was found as oxide layer formers. The amount of NiO is not so significant, reducing that this oxide is practically all distributed in the acid electrolyte. However, unlike titanium where it is possible to manufacture titanium oxide nanotubes, in AISI 304 this becomes more difficult, as each alloy element presents selective dissolution and different speed of diffusion during the oxidation process and subsequent dissolution of the titanium oxides. Consequently, discontinued nanotubes are formed and are randomly distributed on the surface due to differences in the dissolution speed of Ni, Cr and Fe oxides mainly<sup>11</sup>.

The study by Saha et al.<sup>12</sup> evaluated the improvement of corrosive protection in 304 steel for naval applications, in a highly aggressive environment. The authors obtained a nanoporous anodic oxide layer by the electropolishing pretreatment process (in ethylene glycol electrolyte, monobutyl ether and perchloric acid at a voltage of 60 V for 30 minutes) and subsequent anodization with ethylene glycol electrolyte containing 0.1 M of ammonium fluoride and 0.1 M of distilled water at 80 V for 30 minutes. After this process, part of the samples were heat treated in a muffle furnace at 500 °C for 2 hours with a temperature rise ramp of 2.5 °C per minute to minimize the formation of cracks on the anodized surface. This heat treatment is used to remove fluorinated species from the oxide layer. The SEM micrograph of the topography of the sample after heat treatment, showing the formation of pores and a structure that resembles honeycombs. This result should be an electropolishing process that removes the natural chromium oxide passivation layer. Analysis of the chemical composition of the oxide layer indicated that after heat treatment the amorphous oxide was converted into crystalline phase magnetite (Fe<sub>3</sub>O<sub>4</sub>), in addition to the formation of a compact layer of stable thermal magnetite below the porous layer that has excellent anticorrosive properties.

In the study by Doff et al.<sup>13</sup>, on the mechanism of formation and growth of anodic and cathodic films on AISI 316L steel, the authors used an electrolyte of 5 M sulfuric acid at 60°C. Film formation was performed via pulsed square wave polarization with application of 1 pulse every 90 ms for 20 minutes. In the anodic condition, a greater thickness of approximately 200 nm was obtained, while in the cathodic condition, a thickness of 150 nm was obtained.

Burleigh et al.<sup>14</sup> studied using a highly alkaline electrolyte to obtain a nanoporous layer on AISI 1010 carbon steel. A methodology used to obtain this oxide consists of anodization in an electrolyte containing a 12.5 M NaOH solution at elevated temperatures between 50 and 90°C and applied power between 1.6 and 2.6 V for 5 minutes. The authors obtained very overwhelming results regarding

pore formation. Tests were carried out at various electrolyte and tension temperatures, leading to the conclusion that for this process the most important parameters are: applied voltage, electrolyte temperature, electrolyte concentration, electrolyte saturation, thickness of the anode film and the composition of the base metal<sup>14</sup>.

It is observed that there are few studies on AISI 316L to obtain nanotubes. Thus, the objective of this study was to obtain a nanoporous layer by anodizing process on AISI 316L steel in order to achieve improvement on the corrosion resistance for application as metallic biomaterials.

## 2. Experimental

### 2.1. Surface preparation

Shaped plates of AISI 316L stainless steel (medical grade) were used, which were sectioned into pieces of approximately 2.5 x 2.5 cm. The samples were sanded in a bench polisher (Pantec, Polipan-U), following the sequence of 400, 600, 800, 1200, 2400 and 4000 grit sandpaper, finally washed with alcohol and air dried. The pieces were pickled in a 1:3 HF: HNO<sub>3</sub> solution, for 30 seconds, immediately before anodizing. They were subsequently rinsed in water and deionized water, respectively.

### 2.2. Anodizing process

Anodization was carried out using a source of 300V – 500 mA, coupled to a computer for data recording. The sample was connected as an anode a platinum wire was the cathode, 35 mm apart from each other. The process was carried out in galvanostatic mode, with current density of 0.6 mA.cm<sup>-2</sup>. The electrolyte was a 10 M NaOH solution prepared from sodium hydroxide reagent p.a. The anodization was processed at a temperature of 70°C under constant agitation to eliminate gas bubbles<sup>15,16</sup>. Anodization time was 5 minutes<sup>15</sup> and 10 minutes. As there was variation in the color of the samples during anodization for up to 10 minutes, it was decided to also anodize for 10 minutes. The description of the samples is shown in Table 1.

### 2.3. Characterization of the anodized layer surface

The field emission scanning electron microscopy (FE-SEM) was performed in a FEI equipment (Inspect F50) with 20 keV acceleration to evaluate the morphology of the anodized samples. To carry out the crystallographic characterization of the anodic films obtained on the surfaces of the samples, an X-ray diffraction analysis was performed. The X-Ray diffractometer (Shimadzu, XDR-6000) with an X-ray generator using a copper target, with the K alpha radiation of this element (1.5406 Angstrom) and low angle X-Ray beam incidence technique was used. The potentiodynamic

**Table 1.** Definition of sample nomenclatures.

Nomenclature	Description
A-O	Sanded original AISI 316L steel
A-5	Sanded AISI 316L steel and anodized for 5 minutes
A-10	Sanded AISI 316L steel and anodized for 10 minutes

polarization was performed in an AUTOLAB potentiostat (PGSTAT 302). SBF (simulated body fluid) was used as electrolyte in order to simulate corrosive medium<sup>17</sup>. A saturated calomel electrode was the reference electrode and platinum wire was the counter electrode. The scan test used 1 mV/s varying from -200 mV/s to +400 mV/s for the open circuit potential in electrolyte SBF. The open circuit potential of the samples was evaluated in order to follow the corrosion potential value with the exposure time to the SBF solution without the application of electric current, as well as to stabilize this potential for electrochemical impedance spectroscopy tests. Therefore, the OCP values were obtained before the EIE measurements, in the same electrolyte. Electrochemical impedance spectroscopy (EIS) analyses were performed in frequencies ranging from 100 kHz to 3 mHz with 20 mV sinusoidal signal, at each 24 hours for 196 hours. Scanning electron microscopy (SEM) analyses were performed in a JEOL-JSM-6510LV equipment with acceleration voltage of 20 keV to evaluate the formation of corrosion products after electrochemical characterization tests. To make SEM analyses feasible, a thin gold film was applied by plasma magnetron-sputtering. The micrographs were collected in backscattering and secondary electrons modes of detection.

### 3. Results and discussion

#### 3.1. Analysis of anodizing transients

Figure 1 shows the current and potential density transients of the samples anodized in a 10 M NaOH solution electrolyte at 70°C. The sample curves anodized for 5 minutes (A-5) and for 10 minutes (A-10) are shown.

In Figure 1, in the initial seconds of anodization, a current density peak of 0.55 mA/cm<sup>2</sup> and a potential peak of 0.9 V can be observed. These values remained constant until the end of the anodizing process in both analyzed times and were obtained experimentally by optimizing the anodizing parameters such as electrolyte concentration and temperature, potential, current density and sample pre-treatments.

When anodizing with valve metals, the current density drops to almost zero after reaching a constant potential. This behavior is characteristic of the formation of a compact film in which the entire current is used to form it<sup>18</sup>. However, in the case of steel with a predominance of iron and chromium,

this behavior was not observed. The current density, as well as the potential, remain constants at the initial values defined after the experimental evaluation that showed better oxide growth efficiency. This result indicates the occurrence of ionic mobility by a possible mechanism of dissolution-precipitation and oxide growth during the entire process<sup>15</sup>.

Experimentally, the current density and the anodizing potential were increased. However, the system started to prioritize the evolution of oxygen (visual observation of the bubbles formation and electrolyte whitish coloring) to the detriment of the anodic film growth. This movement indicates that the system has moved to a new balance of properties in the transpassive region of iron with potential above 2 V<sup>19</sup>. This low potential value for obtaining an oxide film was also used in a study with 5 M H<sub>2</sub>SO<sub>4</sub> acidic electrolyte in AISI 304 in transpassive region<sup>9</sup>.

The Flade potential of iron (potential in which the passivation region starts) is given around 0.6 V. This value in fact does not correspond to and is higher than the equilibrium potential of any known iron oxide (Fe<sub>2</sub>O<sub>3</sub>, FeO, Fe<sub>3</sub>O<sub>4</sub>), that is, it is not the potential at which the oxide becomes thermodynamically stable. The anodic dissolution of iron is progressively inhibited by changes in the surface and is probably the cause of the observed overpotential. This phenomenon occurs due to the hydrogen depletion process on the charged anode surface. Another possible process is the depletion of hydrogen on the anodic surface carried by the electric current without replacement, which would promote the deposition of Fe(OH)<sub>2</sub> and, in a second moment, the formation of an oxide film by reaction with adsorbed oxygen<sup>19</sup>. In fact, in the results obtained with an average potential of 0.9 V, the formation of an oxide film was observed.

The constant behavior of current density can be explained by the fact that iron dissolution is catalyzed in the presence of OH<sup>-</sup> ions in alkaline solution. This is also observed in acidic solutions even with lower concentration levels of OH<sup>-</sup> ions. The dissolution process has strong involvement of hydroxyl ions, with the initial formation of Fe(OH)<sub>2</sub> or Fe(OH)<sup>+</sup> which quickly decomposes into Fe<sup>2+</sup> in the solution<sup>19</sup>.

Theories of passive film growth mechanisms in stainless steels, such as mixed conduction, include different stages of passive layer formation, starting from the exposed metal surface to the steady state of passivity. The data obtained

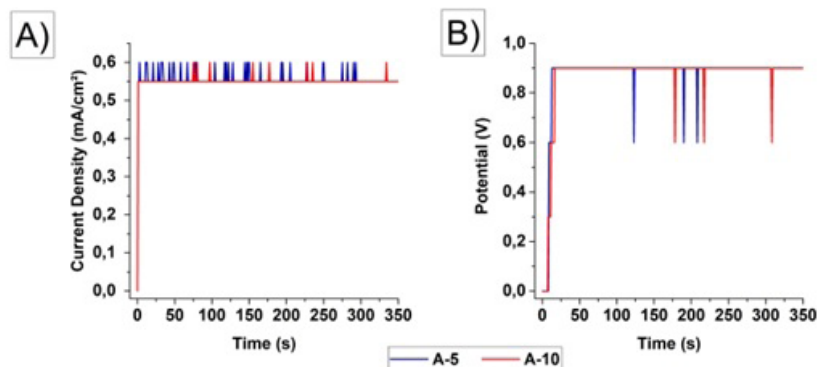
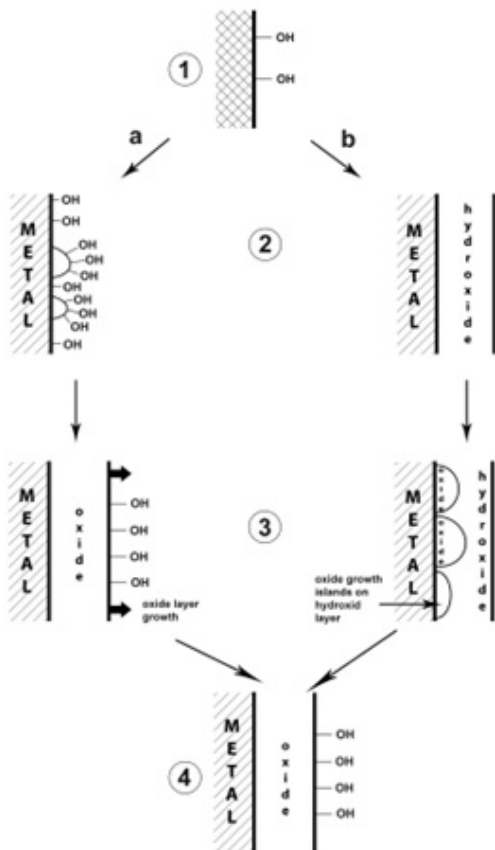


Figure 1. Current density (A) and potential (B) transients of AISI 316L steel anodized in 10 M NaOH solution.

by STM (scanning tunneling microscopy) in borate buffer solution increase the evidence that the formation of passive films undergoes a nucleation process, followed by the growth of the oxide until the formation of a continuous regular film<sup>20</sup>.

Figure 2 illustrate these mechanisms based on classical models and the most recent data, the stages of passive film formation. At point 1 there is a dissociative adsorption of  $H_2O$  or adsorption of  $OH^-$  groups, resulting in surface hydroxylation. Then, the film growth can follow two paths (a or b), depending on the nature of the base metal, the relative stability of the oxides and hydroxides, the pH of the electrolyte, the passivation potential and the temperature.

Path “a” proposes recombination of adjacent  $OH^-$  groups (dehydration) or deprotonation resulting from island formation oxide islands (point 2a). Then, there would be surface hydroxylation and lateral growth of oxide islands to form a complete oxide monolayer with surface hydroxyl groups (point 3a). And finally, there is the growth perpendicular to the surface of an oxide that still presents surface hydroxylation (point 4). In path “b” the growth perpendicular to the surface of a layer of hydroxide or oxyhydroxide completely covering the metal is proposed (point 2b), followed by dehydration or deprotonation and formation of oxide islands in the inner part of the passive film (point 3b) and lateral growth of islands and formation of a complete inner oxide layer under an outer hydroxide or oxyhydroxide layer (point 4). The advancement



**Figure 2.** Proposed mechanisms for initial formation of passive films<sup>20</sup>.

of this reaction can wash to an approximately complete dehydration of the passive film with only but a monolayer of hydroxide or oxyhydroxide remaining on the surface<sup>20</sup>.

The samples after 5 and 10 minutes anodization in a 10 M NaOH solution electrolyte color visibly changes as the anodizing time increases. In sample A-5, the golden-orange coloration indicates an anodic film thickness of approximately 75 nm according to a study that relates the. In sample A-5, the golden-orange coloration indicates an anodic film thickness of approximately 75 nm according to a study that relates the optical refraction index of the oxide with its thickness. Although the study was conducted with AISI 1010 carbon steel, the authors report having observed a similar behavior in the other steel alloys analyzed in a previous study<sup>16</sup>, which is close to the composition of the amount of chromium present in the AISI 316L steel. The golden-orange color is also associated with the greater presence of oxides resulting from the initial substrate dissolution reactions forming iron and chromium hydroxides. In turn, the electrolyte forms the intermediate product ferrite, which oxidizes to form magnetite ( $Fe_3O_4$ ) and hematite ( $Fe_2O_3$ ). The A-10 sample showed a predominantly royal blue color, indicating a greater thickness around 170 nm<sup>15</sup>.

As for the composition of passive films and their relationship with the obtained colors, it should be considered that these films are normally composed of several layers of oxyhydroxides, with composition gradients and the hydration degree in the normal direction to the base metal. According to the double-layer model, the passive film consists of an inner oxide layer and an outer hydroxide or oxyhydroxide layer. For metals with more than one valence, such as iron and chromium, the lower valence ions are usually located in the inner part of the oxide, while the higher valence ones are found in the outer regions of the films<sup>20</sup>. The darker color obtained in the A-10 sample, which was anodized for a longer time, indicates a greater presence of magnetite, an oxide composed of  $Fe^{3+}$  ions, indicating that the ions with higher valence diffused to the outermost part of the film.

This magnetite formation is also related to passive film growth mechanisms. In a study of iron-chromium alloys, the enrichment of chromium in passive films formed in sulfuric acid was verified through XPS analysis and passive current measurements. This behavior was attributed to the preferential dissolution of iron in the electrolyte and the low mobility of chromium in the film<sup>21</sup>. Thus, in the sample anodized for 5 minutes, the yellowish film layer may indicate a greater presence of chromium oxides, while the iron ions are preferentially dissolving into the electrolyte. Over time, the formation of bluish-black iron oxides increases.

### 3.2. Morphological characterization

Figure 3 shows the FE-SEM images of the surfaces for samples A-O, A-5 and A-10 at 10,000, 20,000 and 100,000 magnifications respectively.

The original AISI 316L steel (A-O), which has only been sanded, shows no specific structure, as seen in Figure 3a, b, c. It presents only elongated scratches that are compatible with the lamination process, considering the magnification of the images, to which the original sheet of the samples was submitted. These images indicate that the steel surface

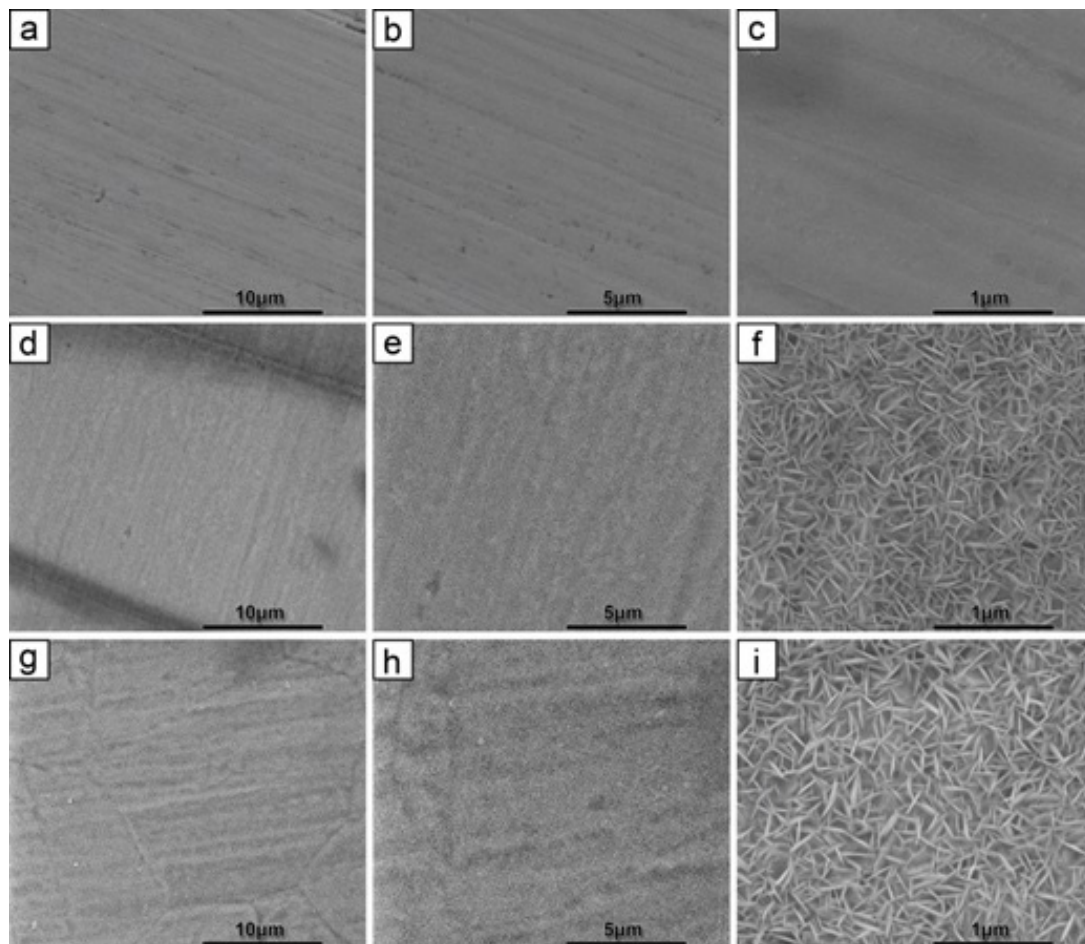


**Figure 3.** Micrographs obtained by SEM in top view of the samples at the following magnifications: (a,b,c) sample A-O; (d,e,f) sample A-5 and (g,h,i) sample A-10 in 10,000, 20,000 and 100,000 times respectively.

is uniform and homogeneous, in agreement with the results obtained for AISI 316L steel without treatments<sup>22,23</sup>. The literature indicates that a thin layer of natural passive oxide is formed, with a thickness ranging from 1 to 3 nm. Due to this very low thickness value it is difficult to identify any structure<sup>23</sup>.

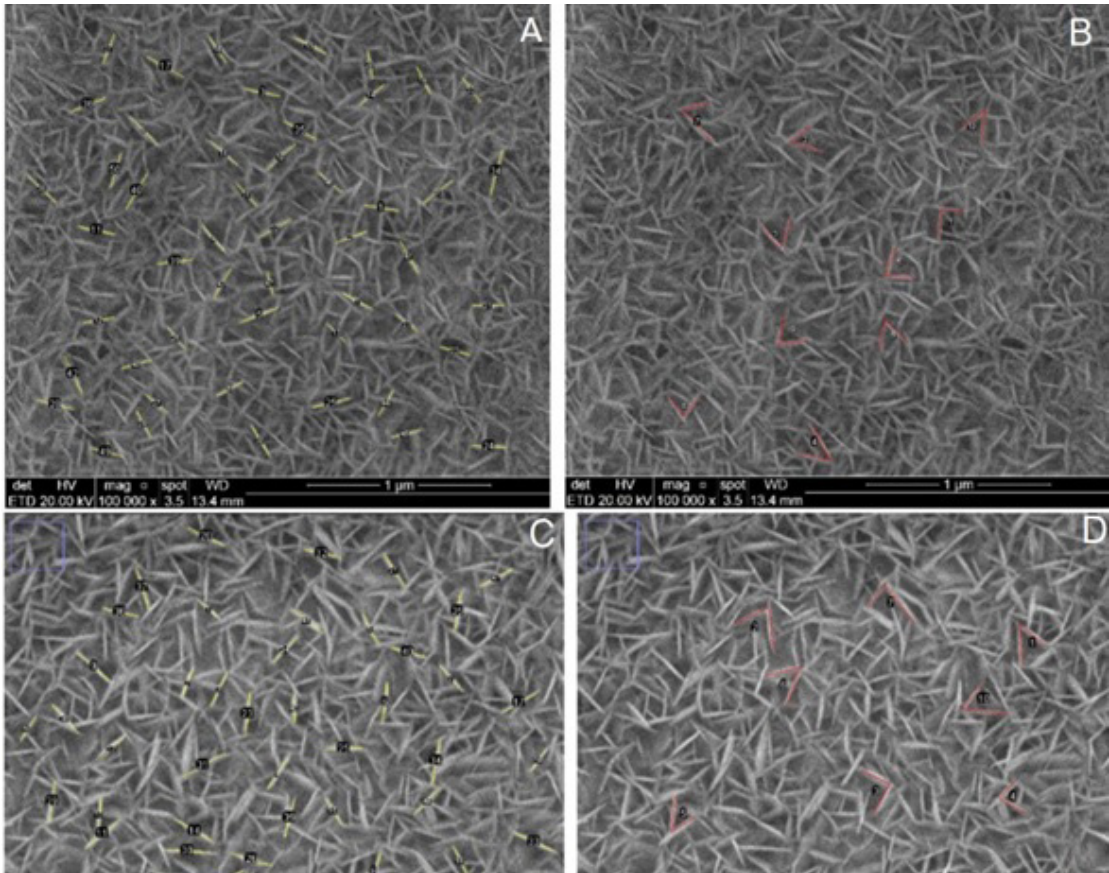
In Figure 3d, e, f, structures formed with an array of nanoplates with well-defined angles can be seen. However, as expected, pores with circumferential openings were not formed, according to the result obtained in the study, which was based on the methodology using 12.5 M NaOH electrolyte and a steel substrate with a low chromium content composition<sup>15</sup>. These differences in relation to our study may explain the differentiated morphology obtained in samples A-5 and A-10. Similarly to sample A-5, sample A-10 (Figure 3g, h, i) showed a subtle difference in the length of the resulting nanoplates, indicating a longer length with a longer anodizing time.

Figure 3d, g, h also shows that the growth of the nanoplates occurs perpendicular to the surface of the grain boundaries due to the predominant mechanism of oxide layer growth is by electrostriction rather than by dissolution-precipitation. If the dissolution-precipitation mechanism were dominant,

it would result in a homogeneous and compact oxide layer, characteristic of barrier-type films<sup>10,15</sup>.

In order to better evaluate the obtained structures, the ImageJ@ software was used as a tool to measure the average length of the nanoplates and the angles formed between them. Figure 4a, b shows the FE-SEM images with the appropriate measurement markings shown in Table 2 for sample A-5.

Figure 4c, d shows the FE-SEM images with the appropriate measurement markings shown in Table 2 for sample A-10. The analysis of the values illustrated in Table 2 shows that the nanoplates in sample A-10 have a greater average length compared to those obtained in sample A-5, indicating that, with a longer anodizing time, in addition to an increase in the thickness of the film layer, the formation by electrostriction seems to maximize. The plaque enlarges until it finds another plaque, thus causing a mutual obstruction on the growth path. At this point, the plaque looks for a new preferred path to continue deposition. A similar phenomenon was observed in the formation of thick nanoporous film in AISI 304 steel. The authors attribute this change in the pore formation path to selective dissolution and random distribution of nickel species present in the substrate. As in this study, the mechanics of porous layer growth in steels is still widely discussed, because



**Figure 4.** Micrographs obtained by SEM in top view of sample (a-b) A-5 and (c-d) A-10 (magnification of 100,000 x) with measurements of nanoplates length and angles between nanoplates carried out in ImageJ@ software.

**Table 2.** Measurements in FESEM top view of samples A-5 and A-10 (magnification of 100,000X) length of nanoplates and angles between nanoplates performed in Image J@ software.

Sample	Average length (nm)	Standard deviation length	Angle between nanoplates (°)	Standard deviation angle
A-5	182.66	25.85	62.99	12.39
A-10	203.63	31.05	63.55	13.92

several alloying elements are present, and therefore many behaviors are presented simultaneously<sup>18</sup>. Nevertheless, we may infer that the heterogeneity in the two cases is caused by physical obstructions of the electrostriction mechanism.

Table 2 shows an angle of approximately 60° between the nanoplates, which refers to the internal angle of the characteristic hexagonal structures of  $\alpha$ -Cr<sub>2</sub>O<sub>3</sub> obtained in tunneling spectroscopy (STM) analysis by Marcus and Maurice (2000) due to the primordial nucleation of oxides on the surface, which possibly influenced the orientation of growth in nanoplate arrays as observed<sup>19</sup>.

### 3.3. Composition characterization

Figure 5 shows the summarized XRD patterns of samples A-O, A-5 and A-10. A reduction in the intensity of the characteristic peaks of the austenitic phase in the anodized samples occurs, and as the anodizing time increases, the intensity reduces more and more, indicating that an oxide film

is formed on the steel surface. A similar effect was observed in the study by Saha et al.<sup>12</sup> on anodic film formation on AISI 304 steel. The steel sample as received only showed the characteristic peaks of the austenite phase ( $\gamma$ -Fe) and the ferrite phase ( $\alpha$ -Fe) as expected. After anodization, the intensity of these peaks reduced, however, without new characteristic peaks, which the authors suggest is related to the amorphous or poorly crystalline nature of the oxides formed in the anodizing process. After the heat treatment of the anodized sample, visible peaks of magnetite phase appear. Therefore, it can be seen in Figure 5 that in the anodized samples the occurrence of the formation of low crystallinity oxides, since only low intensity perturbations are observed along the XRD patterns, but a visible reduction in the intensity of the peaks in relation to the original sample (A-O). This result can also be attributed to the fact that the oxide layer is very thin, as revealed during FE-SEM analysis<sup>24,25</sup>.

In a study by Lin et al.<sup>26</sup>, in which AISI 316L steel underwent alkaline pretreatment with 10 M sodium hydroxide solution, the formation of hydroxyapatite at different temperatures and SBF concentrations was evaluated. The alkaline pre-treatment in question was the immersion of the steel in a 10 M solution of sodium hydroxide at 60°C for 24 hours, then the samples were washed and treated in an oven at 500 to 800°C for 1 hour. In the XRD analysis, the formation of sodium chromium oxide was observed and was an interesting suggestion for the low adhesion of hydroxyapatite due to the low affinity of steel (with metallic bonds) with hydroxyapatite or bone tissue (ceramic material with covalent bonds). Sodium chromium oxide thus plays the role of an interlayer or bridge between the two materials, which would make a big difference to the biocompatibility results, by producing an increase in the surface of hydroxyl groups, which act as nucleation points<sup>19</sup>.

The formation process of the obtained oxide layer nanoplates is illustrated in Figure 6, in addition to the elements present in the substrate. The presence of sodium and oxygen indicates the formation of a compound similar to the one obtained in the study by Lin et al.<sup>26</sup>. It is important to consider that heat treatment was not performed in the current study and some

variations in the crystalline structure are likely to occur. This may be related to the fact that peaks of defined intensity did not occur in the XRD analysis. Figure 6 presents the EDS spectrum of points 1, 2 and 3 with the respective relative weight value of each element at the respective point. Point 3 was selected as the area where nanoplates were not formed. As the result indicates, no sodium was detected at point 3. This leads to strong evidence that sodium participates in the structure that forms the nanoplates.

The results obtained in the XRD and EDS studies are not conclusive enough to state the exact composition of the nanoplates obtained. It is very likely that there are several oxides present in this film due to the nature of the austenitic steel substrate itself and its specific oxidative processes<sup>27,28</sup>.

From the results obtained in the FE-SEM images and in the XRD and EDS studies, a mechanism for the formation of the oxide layer is proposed. The possible process formation of the nanoplates of the obtained oxide layer is illustrated in Figure 7, in which at stage I of the process, the dissolution of ions into the electrolyte occurs simultaneously with the process of adsorption of hydroxyl ions on the metal surface, which already has a thin passive layer of chromium oxide. At stage II, oxide islands are formed by precipitation. Growth of these oxides by processes of dissolution-precipitation and electrostriction is observed at stage III.

### 3.4. Electrochemical characterization.

The results of the polarization curves for the original AISI 316L steel, as well as the samples anodized for 5 and 10 minutes, are shown in Figure 8.

In the polarization curves it is observed that samples of original steel (A-O) and steel anodized for 10 minutes (A-10). Sample A-10 is slightly displaced to the more active region, therefore with inferior anticorrosive properties in relation to A-O. Both show a passivation zone between -0.2 V and 0.2 V right after the corrosion potential, followed by a brief transpassivation zone between 0.2 V and 0.3 V. After, a zone of accentuated activation is seen, which is a characteristic of rupture of passivation, or pitting potential. Afterwards, the current increases was observed constantly, which is inherent

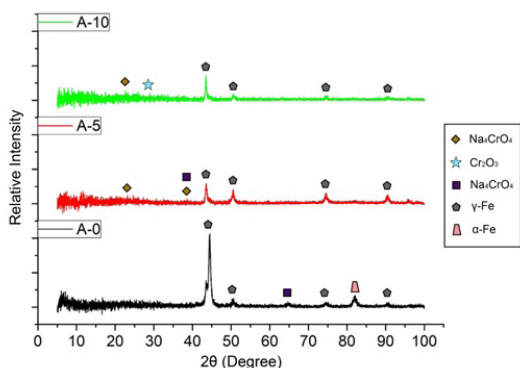


Figure 5. Comparison of the diffractograms of samples A-O, A-5 and A-10.

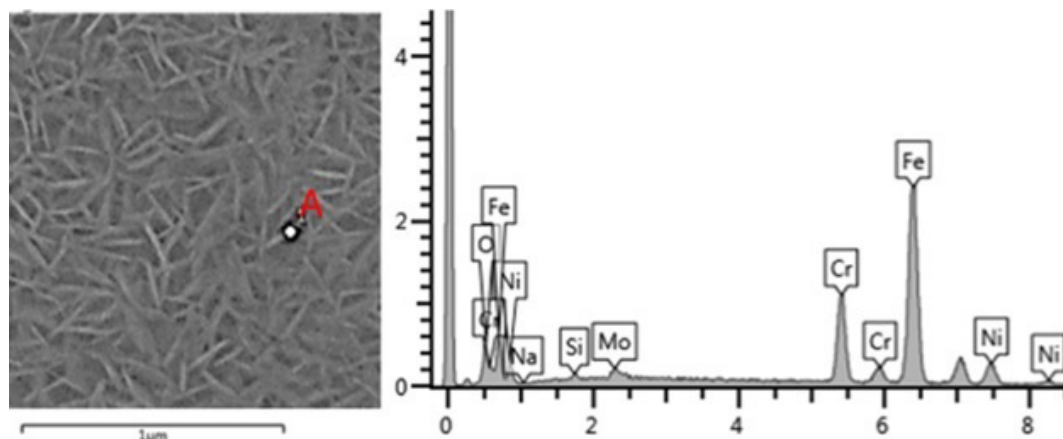
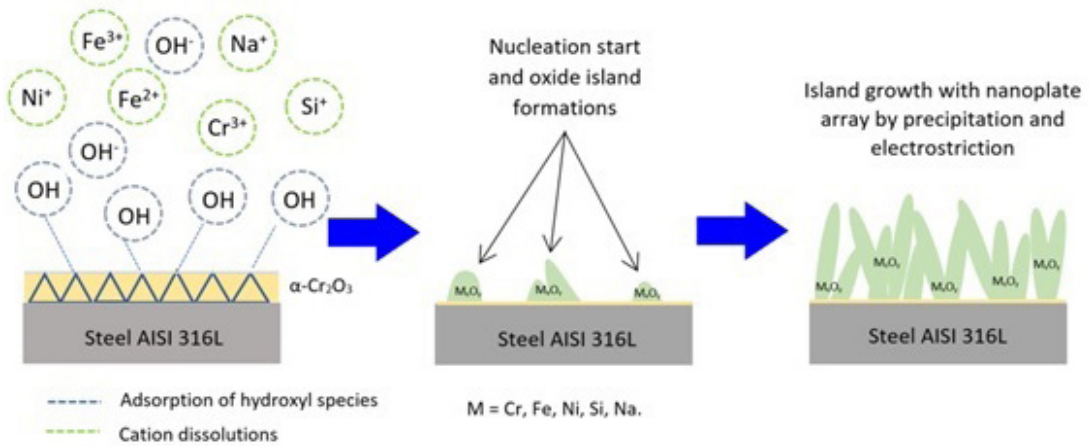


Figure 6. SEM micrograph of sample A-5 with EDS of point A and (b) SEM micrograph of sample A-10 with EDS of points 1, 2 and 3.



**Figure 7.** Possible process of formation of oxide nanoplates.

to the predominance of oxygen evolution<sup>19,20,29</sup>. For sample A-10 the pitting potential was already observed at 0.3 V.

This behavior of sample A-10 is due to its irregular surface. In a study on the properties of nanoporous films obtained by anodizing steel in 50% NaOH, a polarization test in borate buffer solution showed a ratio of increase in the current density proportional to the increase in the anode film thickness. The authors attribute this phenomenon to the fact that the film consists of a porous network of magnetite channels that apparently absorb charge as the oxide alternates between  $\text{Fe}^{2+}$  and  $\text{Fe}^{3+}$ <sup>16</sup>.

A marked decrease in the corrosion current density for sample A-5 can be seen. The behavior also differs from samples A-O and A-10, as its curve does not have a transpassivation zone, that is, it only presented a passive behavior during the test, showing the greater protective action of this film in relation to other samples and consequently this film allows the implants to have a long life<sup>21,30</sup>.

Table 3 presents the parameters obtained by the Tafel extrapolation of the curves. The corrosion potential ( $E_{\text{corr}}$ ) and corrosion current density ( $i_{\text{corr}}$ ) parameters are the intrinsic factors to determine the ability to inhibit the corrosion degradation of a protective layer. A protective layer has better corrosion resistance when more positive corrosion potential values and lower corrosion current values are obtained<sup>16</sup>. These data suggest that the A-5 sample has a superior corrosion resistance property than the original steel (A-O). However, the A-10 sample anodized for a longer time did not have the proportional response, and its result was more inferior than that of the original steel.

An interesting fact that should be pointed out is the application to which the material is intended to be used. Studies of anodized steels in a mixture of ethylene glycol, ammonium fluoride and water for marine applications (highly aggressive environment due to the presence of chloride ions) show that a thermally treated nanoporous layer presents nobler potentials than the original steel<sup>26</sup>. The authors attribute this effect to the mechanism of preventing the arrival of ions on the surface of the base metal provided by the compact barrier layer of thermal oxide. Contrary to what was shown in this study, the sample with greater porosity showed fewer noble values compared to the original steel.

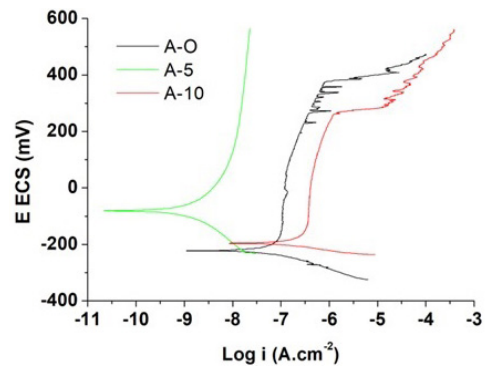


**Figure 8.** Representation of the polarization curves for the original AISI 316L steel samples, anodized for 5 and 10 minutes in 10 M NaOH solution.

**Table 3.** Potentiodynamic polarization parameter obtained for A-0, A-5 and A-10 specimens in SBF.

System	$E_{\text{corr}}$ (mV)	$i_{\text{corr}}$ ( $\text{A}\cdot\text{cm}^{-2}$ )
A-O	-223.1	$2.55 \times 10^{-8}$
A-5	-79.8	$1.02 \times 10^{-9}$
A-10	-195.5	$4.64 \times 10^{-8}$

It is a relevant fact that for biomaterials, the electrolyte (SBF) also contains aggressive ions such as chloride, but in smaller amounts. Thus, it can be interpreted that one should work with an ideal value for the thickness of the nanoporous layer for application in biomaterials, seeking an optimization that considers corrosion protection and simultaneously presents favorable aspects to osseointegration<sup>13,31</sup>.

Figure 9 illustrates the SEM top views for the A-O, A-5 and A-10 samples after potentiodynamic polarization test in SBF solution. By macroscopic observation it was not possible to detect corrosion products in any of the samples. In the SEM image shown in Figure 9, the formation of whitish crystals can be seen, possibly originating from salts

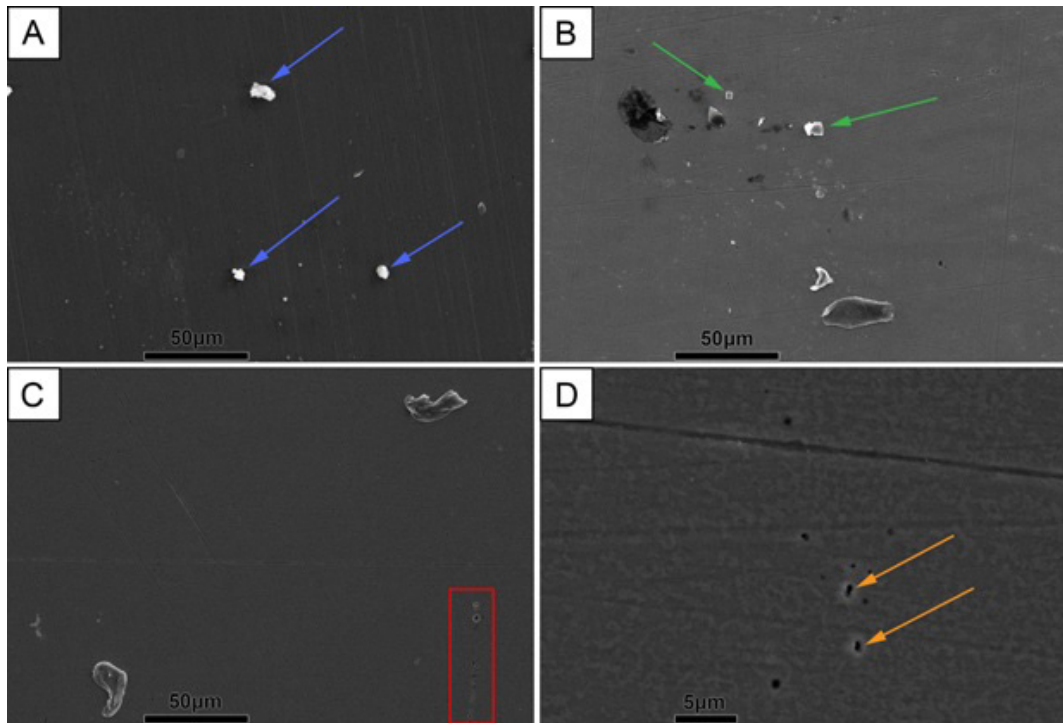


**Figure 9.** Micrographs obtained by SEM after polarization test potentiodynamics in SBF for samples A-0 (A), A-5 (B), A-10 (C) and emphasis enlarged sample A-10 (D).

dispersed on the surface in all samples. Figure 9a crystals are shown with blue arrows and in Figure 9b with green arrows. Specimens A-0 and A-5 showed similar results. Figure 9b evidences the formation of crystals with a well-defined cubic geometry being, possibly, sodium chloride crystals as the SBF electrolyte has chloride ions in its composition. This type of formation was also observed in carbon steel samples simulated in a hot oxidation environment in the presence of  $H_2S$  and  $CO_2$  gases and 3.5% sodium chloride solution. The formation of these crystals can increase the risk of pitting initiation by degradation of the passive layer of AISI 316L stainless steel<sup>32,33</sup>.

In Figure 9c, the formation of superficial crystals is also observed, however, the capture of several punctiform formations is noteworthy (highlighted in the box in red). In Figure 9d, an increase in these formations was observed, indicating the occurrence of pits, which agrees with the polarization curve obtained for this sample, which presented an early passivity rupture in relation to samples A-0 and A-5. The most favorable conditions for good passivation are those in which the alloy surface is free from any contamination and the exposure medium is oxidizing. However, if the passive layer is damaged and the environment conditions do not allow repassivation, corrosion rates can be high<sup>21</sup>.

Figure 10 shows the results of the OCP tests of the samples of A-0, A-5 and A-10. The three samples showed similar values during OCP monitoring, especially after the 48 hours of immersion in SBF. This indicates that, over time, the anodized layer no longer influences the metallic substrate as a protective physical barrier, and that the corrosion products formed have a greater predominance in

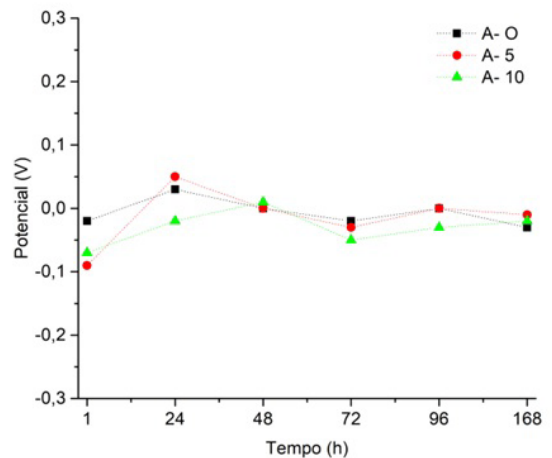


**Figure 10.** Open circuit potential measurements for the original AISI 316L steel samples, anodized for 5 and 10 minutes.

the events of electrochemical reactions. The anodized samples (A-5 and A-10) assume a similar character to the behavior of the original 316L steel (A-0) in terms of electrochemical activity. This fact can be taken as positive, as AISI 316L stainless steel is known for its good resistance to corrosion allowed by the formation of an adherent passive oxide film and which provides the material a certain stability against corrosive action<sup>34</sup>. It is also known that austenitic steels owe their corrosion resistance to the spontaneous formation of a surface protective film of chromium oxide adhering to the

metal surface, acting as a barrier, inhibiting the corrosion process and keeping the release of ions at very low levels<sup>35</sup>. However, the objective of this study is to obtain a surface that can be used as a biomaterial with a positive balance in terms of corrosion resistance and bioactivity.

Distinct phenomena between samples can be observed in the measurement after 1 hour of immersion in SBF. The original steel sample has a higher potential value, that is, it is less active, in relation to the anodized samples, indicating that the natural air-formed passive layer is acting satisfactorily. The natural chromium oxide formed in AISI 316L steel is characteristic of the amount of chromium presented as an alloying element. The mechanism of formation of this layer is based on the ability of chromium ions to migrate to the active regions of grain boundaries, thus having its preferential oxidation to iron, which enhances its protective action against corrosion<sup>21</sup>. Anodized samples, despite having a lower potential ( $\sim -0.08V$ ) not so discrepant in relation to the original steel ( $\sim -0.02V$ ), present values up to 0.05V.

The A-10 sample presented a lower potential than the A-O sample after 1 hour of immersion. More porous surfaces favor the permeability of the electrolyte through the anodized layer, and this in turn contributes to a lower resistance to metal corrosion<sup>26</sup>. An explanation to the lower potential of anodized samples after 1 hour of immersion may be related to the highly active surface, the plentifulness of hydroxyl free radicals at the surface<sup>20</sup>. This is proposed in the passive film formation mechanism. These free radicals can favor the reactions with the ions of the SBF solution at the initial moment of formation of the electric double layer.

After 24 hours of immersion, a change in the condition of sample A-5 is observed, with a more noble potential than the original AISI 316L steel. This indicates that the anodized layer obtained in this sample has superior protection characteristics than the original steel (A-O). Steels anodized for less time generated thinner and more adherent oxide layers due to the greater presence of chromium<sup>15</sup>. Likewise, these more adherent layers also showed more satisfactory results in corrosion resistance tests. The XRD analysis shows that the sodium or potassium cations present in the electrolyte also can be observed in the anodized layer. Therefore, it is possible to consider the formation of sodium chromium oxides, in addition to the expected chromium iron oxides and iron oxides. The presence of this type of stable chromium-sodium oxide in addition to the protective natural chromium oxide showed good corrosion resistance results in studies using SBF and saline water<sup>15,24,36,37</sup>.

The A-10 sample still presented a lower potential result than the other samples at 24 hours of immersion, indicating inferior corrosion resistance properties. This is in accordance with the result obtained in the polarization. This behavior is linked to the fact that this anodized layer, despite having a greater thickness, is formed by many low-adherence iron oxides such as maghemite ( $\gamma\text{-Fe}_2\text{O}_3$ ) and hematite ( $\alpha\text{-Fe}_2\text{O}_3$ ) instead of being constituted preferentially by magnetite (cubic- $\text{Fe}_3\text{O}_4$ ) which is more adherent and has a higher corrosion resistance capacity<sup>15</sup>.

Figure 11 shows the results obtained by the electrochemical impedance test of the A-O sample, after 168 hours of immersion in the SBF solution in the two representations of the Bode plot.

The original steel sample exhibited the known passivity characteristics of the 316L stainless steel attributed to a very thin natural bonded chromium oxide layer. In the scan, after 1 hour of immersion in the SBF solution, the usual behavior of passivable metals was noted. At a high frequency, the resistance of the solution was predominant, evidenced by the practically null phase angle. This purely resistive behavior can be attributed to the ohmic resistance of the SBF solution<sup>38</sup>. The system is constant from high to medium frequencies at values close to  $50^\circ$ , indicating permeability through the oxide layer. At a low frequency the phase angle reduces to values around  $38^\circ$ , indicating the occurrence of corrosive processes in the metal substrate. This behavior after 1 hour of immersion is related to the presence of chloride ions in the SBF solution, which are very damaging to the steel and responsible for increasing the corrosion rate of the material<sup>26</sup>.

After 24 hours of immersion, the curve behaves similarly to the 1-hour scan. However, with a slight shift to lower phase angle (around  $30^\circ$ ) at low frequency. This fact indicates that more resistive corrosion products were formed at the oxide/metal interface and that reactions governed by mass transfer were more predominant than charge transfer reactions.

After 48 hours of immersion, the sweep curve changes significantly, possibly due to the formation of corrosion products of a resistive nature and the regenerative ability of the passive chromium oxide layer of stainless steels<sup>39</sup>. At a low frequency, the resistive behavior remains stable at values from  $25^\circ$  to  $30^\circ$ . In medium to high frequency, a resistive constant appears, indicating a kind of blocking of the passive layer for charge transfer and predominance of mass transfer, shifting the charge transfer to the oxide/electrolyte interface. This behavior favors the corrosive protection of the metal and justifies the higher impedance modulus (Figure 11) than the results of 1 and 24 hours. A similar behavior was obtained in coated systems that denote superior corrosion protection in relation to the temporary protection promoted by oxides<sup>40</sup>.

However, after 72 hours of immersion, the profile of the protective system of the metallic substrate changes. It is related to the limit of permeability through the corrosion products that they temporarily protect. A highly capacitive behavior is observed at low and medium frequencies, with a phase angle around  $80^\circ$  denoting permeation of the passive layer and formation of corrosion products at the metal/oxide interface. In the  $\text{Log}|Z|$  graph, the total resistivity of the system drops sharply in relation to previous scans, indicating an increase in the transfer of loads at low and medium frequencies. This instability in the protection of the natural passive oxide layer of stainless steel was also observed in studies by Giordano et al.<sup>27</sup>. In the study, the authors attribute this behavior to the characteristic of austenitic stainless steels that present pitting corrosion and can repassivate them, as observed in the SEM images of the study. The behavior of the polarization curve corroborates the appearance of pitting corrosion in the A-O sample, due to the sudden increase in the current density of the anode curve. At 96 hours of immersion, the same behavior can still be observed without any noticeable changes<sup>36</sup>.

At the last moment, the sample was left in immersion for a period of 168 hours. In this scan, the resumption of the similar behavior presented at 1 and 24 hours of immersion

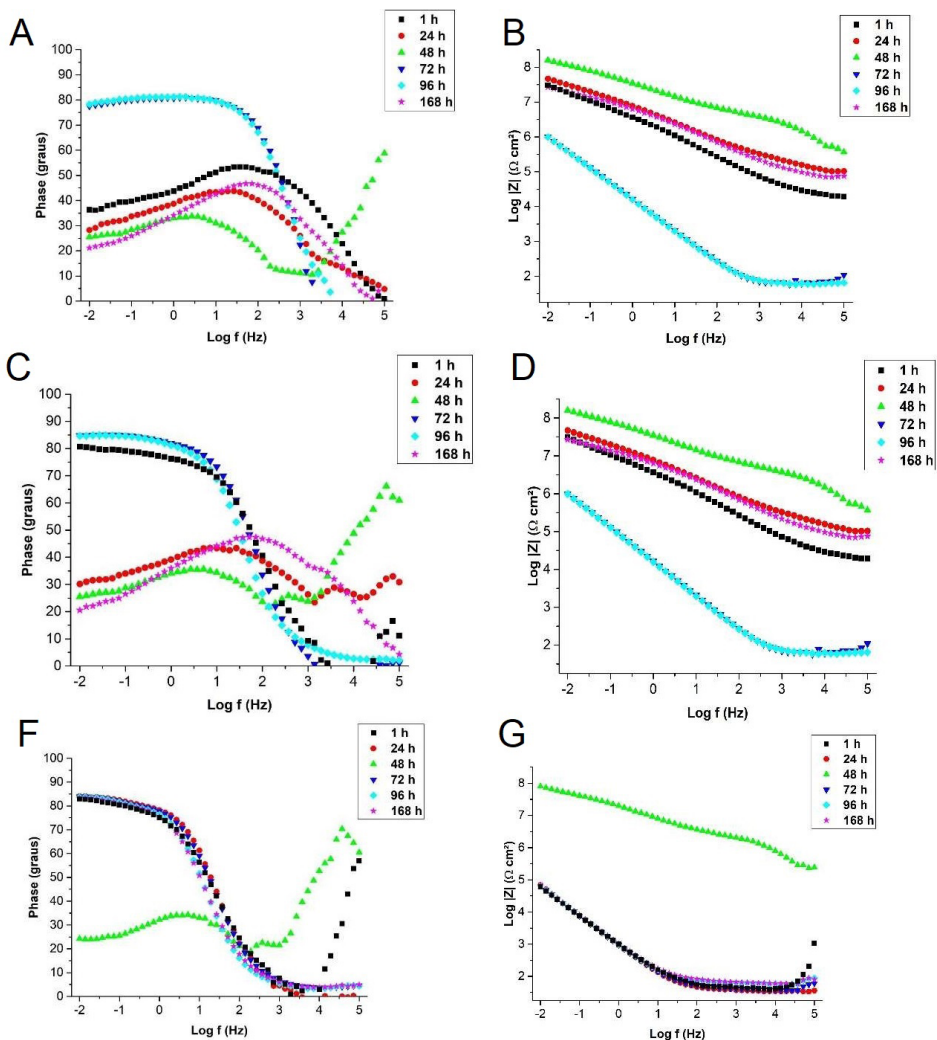


**Figure 11.** Bode EIE plots (a) phase angle, (b) modulus of impedance for original steel sample (A-O), (c) phase angle, (d) impedance modulus for steel sample anodized for 5 minutes in 10M NaOH electrolyte (A-5), (e) phase angle and (f) module of impedance for steel sample anodized for 10 minutes in 10M NaOH electrolyte (A-10).

was observed. This result is expected for a stainless steel. The passive layer clearly regenerates, confirming the excellent anticorrosive properties of AISI 316L steel<sup>35</sup>. But it is important to note that the phase angle at a low frequency resulted in a lower value, around 20°, indicating that the new metal/oxide interface layer is different from that observed at 1 hour. In this case, the corrosion products were incorporated into the metal and oxide interfaces, altering the behavior in relation to the original passive layer<sup>24</sup>. Figure 11 shows the results obtained by the electrochemical impedance test of the steel sample anodized for 5 minutes in 10M NaOH electrolyte (A-5), performed for a period of 168 hours of immersion in the SBF solution in the two representations of the Bode diagram. The A-5 anodized sample showed, in general, a similar behavior to the original steel (A-O), mainly after 24 hours of immersion in SBF. The scan is different after 1 hour of immersion, that is, right at the beginning of the analysis. At a low frequency, the sample presented a phase angle around 80°, remaining in this

capacitive behavior in the passage from a low to a medium frequency, denoting permeability of the electrolyte. Indeed, this fact reveals the presence of an oxide layer with different characteristics from the natural oxide layer present in the original steel. This fact corroborates the result obtained in the OCP analysis, which presented a lower initial potential than the original steel. In turn, in the contact angle test, sample A-5 presented hydrophilicity superior to the original steel, which may suggest that it does not have porosity that justifies this permeability behavior of the electrolyte that is so pronounced at 1 hour of immersion. This intense activity in the initial period at the metal/oxide interface is possibly attributed to the anodized surface that starts to present a high number of free hydroxyls due to the characteristic of the electrolyte used in anodizing<sup>20</sup>. These hydroxyl radicals attract the ions from the SBF solution, making the oxide layer more permeable. The oxide layer obtained in sample A-5 is constituted of a greater presence of chromium and sodium. The presence of sodium in the oxide layer can be correlated

with studies of silver addition in zirconia-based protective films on 304L steel. In this study, the incorporation of Ag decreases the corrosion resistance due to the increase in the electrochemical activity of the ceramic film, provides the incidence of increased active sites in the protective layer and increases permeation paths of the electrolyte solution due to the increase in the contours of grains<sup>41</sup>.

After 24 hours of immersion in SBF, the A-5 sample already presented a similar behavior to the original steel sample (A-O). This can be attributed to the now added strength of the corrosion products formed at the metal/oxide interface. Differently from the A-O sample, high-frequency coupled events are observed, therefore indicating the presence of a slightly capacitive activity at the oxide/electrolyte interface. Hence, some alteration in this region may be attributed to the formation of ceramic compounds, such as hydroxyapatite, by reaction of hydroxyl free radicals with ions from the SBF solution. Lin et al.<sup>26</sup> observed a greater deposition of hydroxyapatite on AISI 316L steel with alkaline pretreatment. Figure 11f shows the results obtained by the electrochemical impedance test of the steel sample anodized for 10 minutes in 10M NaOH (A-10) electrolyte, performed for a period of 168 hours of immersion in the SBF solution in the two representations of the Bode diagram.

Sample A-10 showed a clearly different behavior compared to samples A-O and A-5. A highly capacitive behavior at low frequency with a phase angle around  $83^\circ$  is noticeable early, after 1 hour of immersion. It is observed in sample A-5, however, when scanned after 24 hours of immersion, sample A-5 already shows similar behavior to the sample A-O, while for the sample A-10 the initial behavior is repeated. This suggests that corrosion product formation reactions are still taking place at the metal/oxide interface. This phenomenon agrees with the behavior of iron oxides, which were formed in this study, such as hematite and maghemite. These oxides provide greater permeability of the anodized layer<sup>16</sup>. This greater permeability of the electrolyte also corroborates the contact angle analysis, suggesting a more porous surface composed of low-adherence oxides. Permeability events are observed through the anodized layer in regions of medium frequency. This initial higher surface activity corroborates the results obtained for sample A-10 regarding the open circuit potential. Looking at the  $\log|Z|$  it can be concluded that this sample, even with a similar behavior to sample A-5, has a lower corrosion resistance, as the total impedance is reasonably lower than the values presented by samples A-O and A-5.

In the scan after 48 hours of immersion, similarly to the other samples, the protective behavior resulting from the predominant action of the formed corrosion products can be noted. There is an intense increase in the total impedance of the system and low frequency phenomena starts to present a predominance of the resistive character observed by the phase angle at approximately  $25^\circ$ . Also according to sample A-5, this now presents a constant on average for a high frequency, indicating the formation of some barrier product that induces capacitive behavior at the oxide/electrolyte interface. The formation of corrosion products with provisional capacity for corrosive protection is very common in steel and aluminum alloys. A certain amount of metal ions responsible

for the formation of oxide are still available and these will preferably be responsible for increasing the total impedance of the system, mainly due to the resistance imposed to the permeation of electrolyte over time<sup>42</sup>.

As observed in all samples, this protective limit reaches a saturation after 72 hours of immersion in the SBF. The same behavior occurs with constant return at a low frequency of highly capacitive behavior. However, in the same values obtained in 1 and 24 hours of immersion, a lower total impedance is once again observed, unlike in samples A-O and A-5.

Contrary to what was observed in the other samples, the A-10 sample failed to recover the initial behavior after 168 hours of immersion. The sample maintained the behavior observed after 72 hours of immersion and this can be related to the type of corrosion product formed, with low adhesion and greater permeability. The excessive permeability of the anodized layer, in this case, proved to be negative from the point of view of corrosion resistance, denoting the need for some barrier in order to slow down the permeation process. The importance of a barrier layer in the metal coating was noted in the study by Saha *et al.*, (2019)<sup>12</sup> when evaluating original AISI 304 steel, anodized and anodized and heat treated. The authors evidenced a superior corrosion resistance performance of the heat-treated anodized steel as a compact thermal oxide barrier layer was obtained inside the porous anodized layer. This thermal oxide layer is responsible for the significant decrease in the corrosion rate evidenced by the polarization resistance values. The only anodized steel had a lower result than the original steel, a fact that the authors relate to the porosity of the oxide layer that favors the permeability of the electrolyte compared to the protective oxide formed in the air present in the original steel.

This result of sample A-10 confirms the higher corrosion current density found in the polarization curves (Figure 11), imparting a lower corrosion resistance to this sample. In biomaterials, this aspect can cause inflammation problems in the human body due to surgery or injury, since this scenario leads to a drop in the pH of the body fluid in regions close to the implant, due to the secretion of inflammatory cells<sup>5</sup>.

Figure 12 shows the SEM images for the sample of sanded original steel (A-O) after an electrochemical impedance spectroscopy (EIS) test for 168 hours of immersion in the SBF solution. Corrosion products were not visually detected after the EIS in the evaluated metallic substrates or alterations in the surfaces of the 3 analyzed systems. In the SEM images obtained from the area in contact with the electrolyte, whitish crystals appear, possibly due to corrosion products, such as oxides dispersed on the surface. Figure 12b shows the SEM view for the 5-minute anodized steel sample in a 10M NaOH solution (A-5) after the electrochemical impedance spectroscopy (EIS) test for 168 hours of immersion in the SBF solution.

Similarly to sample A-O, sample A-5 also showed whitish crystals, possibly due to corrosion products such as oxides dispersed on the surface. This was expected given the EIS results with similar behavior from samples A-O and A-5. The EDS analysis shows an alteration in relation to the A-O sample, in which the most accentuated presence of silicon, sodium and oxygen is now found, in addition to the atoms

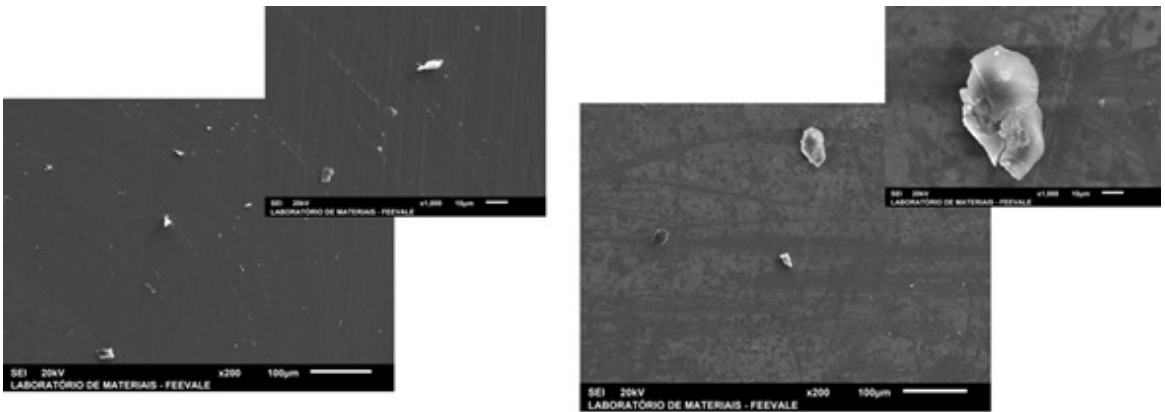


Figure 12. Micrographs obtained by SEM after EIE (a) sample A-O and (b) sample A-5.

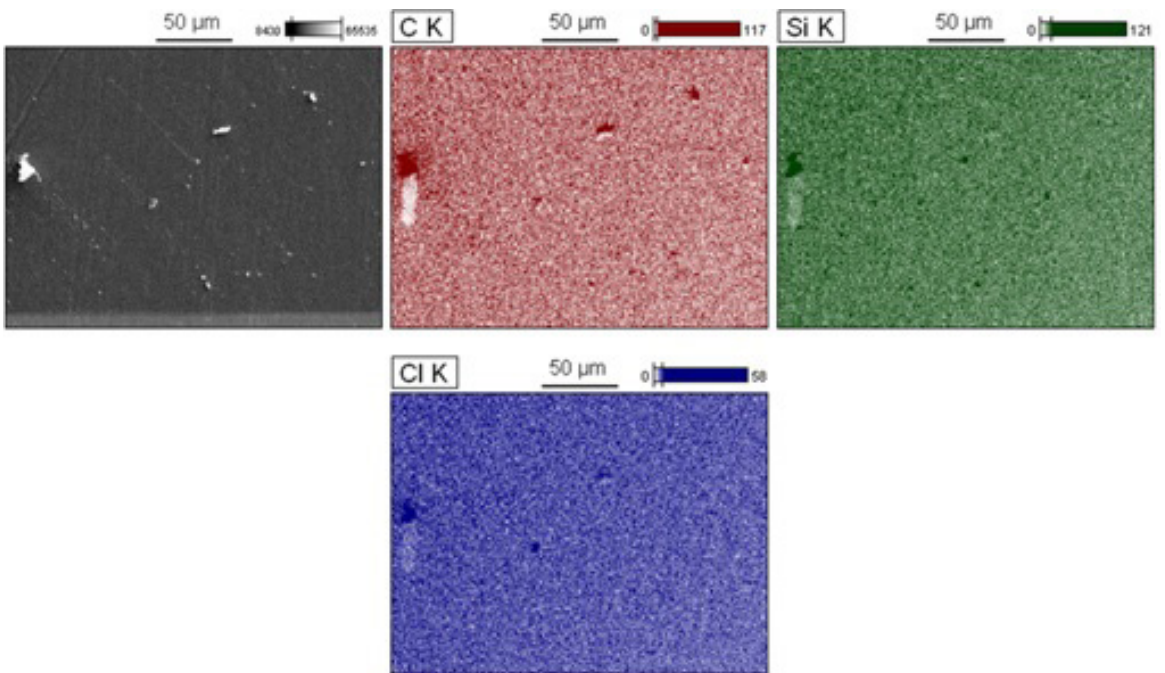


Figure 13. EDS mapping after EIE for sample A-5.

observed in the A-O sample, both in the composition of the crystals and on the surface. This is related to the anodized layer of the surface, due to the anodizing characteristic in NaOH solution and the formation of oxide caused by the growth of the passive layer. The interaction of the sodium ion in the reactions is evidenced by its presence in the anodic film<sup>16</sup>.

Figure 13 illustrates the EDS chemical mapping with the purpose of investigating the composition of the crystals observed on the surface. The image shows the mappings obtained from the atoms with greater intensity in the points of interest. These crystals are mainly composed of carbon, silicon and chlorine atoms, denoting the interaction of salt ions present in the SBF electrolyte, especially the chloride that acts more acutely

in corrosive processes<sup>32</sup>. The Silicon element is probably present due to the sanding process. The low incidence of corrosion products observed was expected because after 168 hours of immersion the sample has a phase angle of  $\sim 20^\circ$  at a low frequency.

The formation of these crystals as a result of the type of electrolyte used may be responsible for future heterogeneities responsible for the initiation of harmful corrosive processes.

Figure 14 shows the EDS scanning of an observed crystal indicating silicon and chlorine as the major constituents.

Figure 15 shows the SEM image for the 10-minute anodized steel sample for 10 minutes in a 10M NaOH solution (A-10) after an electrochemical impedance spectroscopy (EIS) test for 168 hours of immersion in the SBF solution.

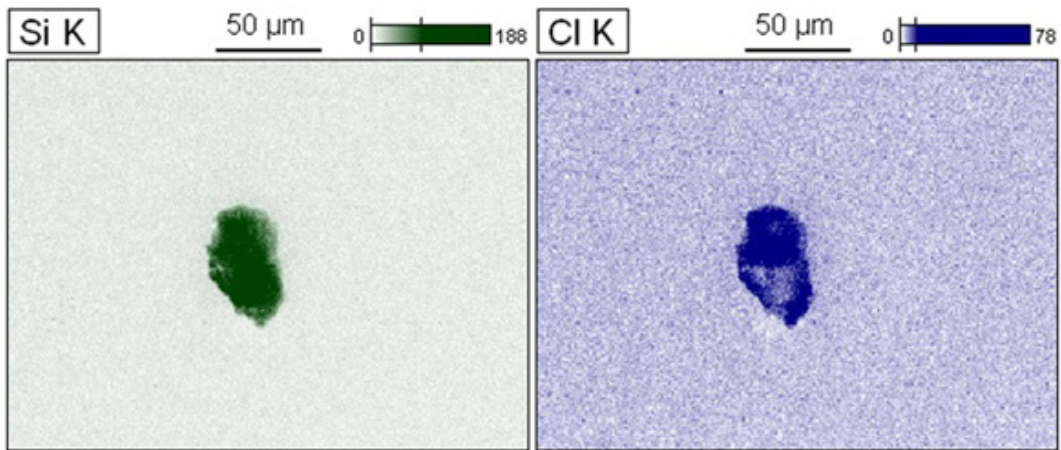


Figure 14. EDS mapping after EIE for sample A-10.

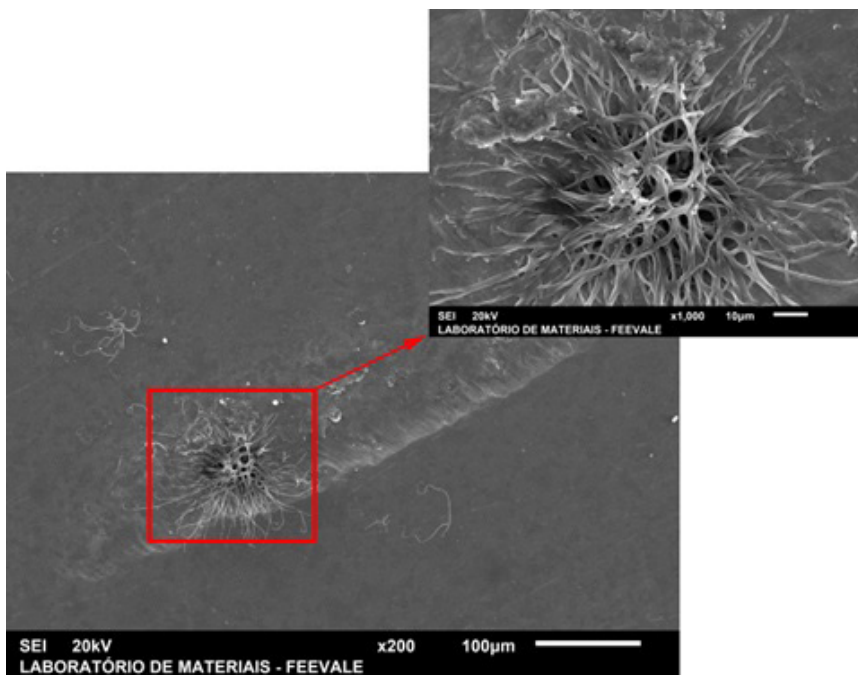


Figure 15. Micrographs obtained by SEM in top view of sample A-10.

The sample A-10 did not show, macroscopically, visible corrosion products. However, in the SEM view (Figure 15) filiform formations with a branched aspect were observed. The appearance of these corrosion products is consistent with the results obtained in the potentiodynamic polarization and EIS tests, in which sample A-10 showed lower yield in terms of corrosion resistance compared to samples A-O and A-5.

As verified in the Bode curves (phase) for sample A-10, after 168 hours of immersion in SBF, a phenomenon at low frequency is verified, with an angle close to  $90^\circ$  associated with the permeability of the electrolyte through the anodized layer.

Figure 16 shows the EDS chemical mapping of the filiform formation observed in sample A-10.

As a result, the main constituent element of the outcrop is carbon. This type of corrosion product is not very common in steel due to its low carbon content. Graphitic products are normally present in a type of selective corrosion called filiform graphitization, which is recurrent in gray cast iron. The most common cause is due to any initial heterogeneity, causing the oxidation of iron. The graphite (carbon) remains unchanged, thus forming a Fe/Graphite pile, in which the graphite behaves like a cathode in relation to the metallic matrix<sup>24,29,41</sup>.

The appearance of this type of corrosion product, by the mechanism described for gray cast iron, may be possible because the A-10 sample has shown greater porosity and

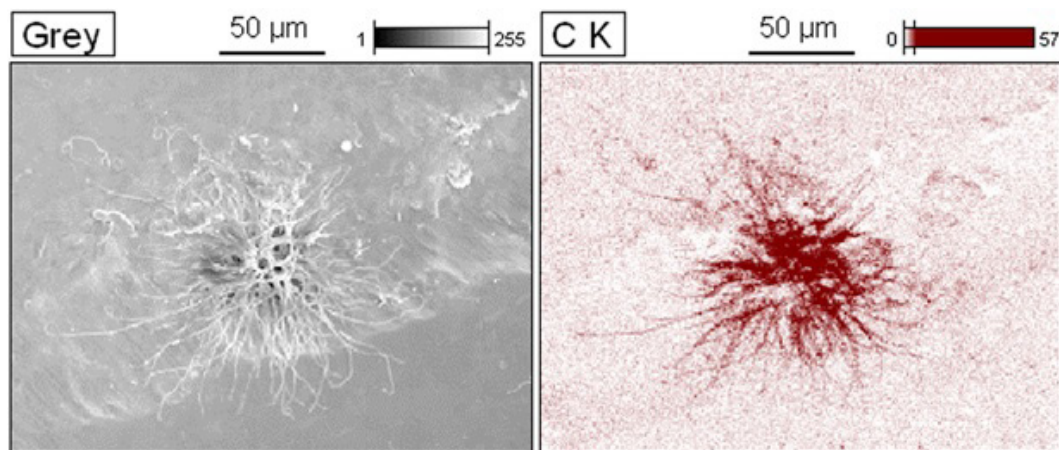


Figure 16. EDS mapping after EIE for sample A-10.

hydrophilicity in the contact angle test and by the color analysis. Thus, possibly, the anodized layer is constituted of less adherent iron oxides. This high amount of iron oxides allowed the formation of free-state carbon micronuclei on the surface, starting the growth in the form of continuous branches, as evidenced in the micrographs of sample A-10. The presence of carbonates in the SBF electrolyte must also be considered, which may have an interaction when in a dissociated form contributing to the observed carbon outcrops<sup>38</sup>.

In general, sample A-5 presented the most satisfactory results, being very close to the behavior of the original stainless steel AISI 316L, which in itself is a material with excellent corrosion resistance properties. Sample A-5 showed a better result in the potentiodynamic polarization test, but in the EIS test its performance was slightly lower than the original steel sample (A-O) in terms of the regeneration capacity of the passive layer.

Assessing biomaterials regarding their behavior in a corrosive environment is essential, given that after the implantation of an orthopedic device, an inflammatory reaction is initiated both in response to invasion due to the procedure, and the presence of the device as a foreign body to the body. This reaction results in the production of reactive oxygen species by macrophages, neutrophils and other cells due to an inflammatory response. There is a local increase in the concentration of hydrogen peroxide, neutrophils produce lactic acid leading to an increase in acid pH at the interface between the medium in which the biomaterial is inserted<sup>42</sup>.

#### 4. Conclusion

The results discussed above show that it is possible to obtain a nanorugous layer, with nanoplate arrangement, in AISI 316L steel by the anodizing process in a 10M NaOH electrolyte. The XRD and EDS studies were not conclusive enough to prove the composition of the oxides forming the nanoplates, indicating that, supposedly, the nanoplates are formed by low crystallinity oxides with the presence of chromium, iron, nickel and sodium. The formation of the anodized layer occurs through a process of formation of the nanoplates, in three stages according to the proposed process.

Initially, at stage I of the process, the dissolution of the ions into the electrolyte occurs simultaneously with the process of adsorption of hydroxyl ions on the surface of the metal, which already has a thin passive layer of chromium oxide. At stage II, the formation of islands of oxides begins followed by precipitation and growth of these oxides by processes of dissolution-precipitation and electrostriction, at stage III. The layer obtained with an anodizing time of 5 minutes presented anticorrosive protection efficiency when in contact with body fluids, denoting good corrosion resistance. Consequently, the leaching of dissolved ions by the human body is reduced. The anodized layer had good electrochemical performance, indicating greater polarization resistance and high impedance modulus, with no loss of anticorrosive properties compared to the original steel sample. The layer obtained therefore, a promising alternative for future applications in biomedical areas, especially in orthopedic implants, when comparing the results with the original AISI 316L stainless steel sample.

#### 5. Acknowledgments

This work was carried out with the support of CNPq, a Brazilian government entity focused on training human resources. The authors also thank the financial support of Brazilian agencies: FAPERGS and FINEP. The authors would like to thank the Coordination for the Improvement of Higher Education Personnel - Brazil (CAPES/PROEX 88881.844968/2023/1061/2023) for financial support.

#### 6. References

1. Brasil. Departamento de Informática do Sistema Único de Saúde – DATASUS [homepage on the Internet]. Brasília: Ministério da Saúde; 2020 [cited 2020 Mar 5]. Available from: <http://datasus.saude.gov.br/>
2. Chen Q, Thouas GA. Metallic implant biomaterials. *Mater Sci Eng R Reports*. 2015;87:1-57. <http://doi.org/10.1016/j.mser.2014.10.001>.
3. Moraes LFS, Silva EN, Silva DAS, de Paula PA. Gastos com o tratamento da osteoporose em idosos do Brasil (2008-2010): análise dos fatores associados. *Rev Bras Epidemiol*. 2014;17:719-34. <http://doi.org/10.1590/1809-4503201400030012>.

4. Pinheiro MM, Ciconelli RM, Jacques NO, Genaro PS, Martini LA, Ferraz MB. O impacto da osteoporose no Brasil: dados regionais das fraturas em homens e mulheres adultos: the Brazilian Osteoporosis Study (BRAZOS). *Rev Bras Reumatol*. 2010;50(2):113-20. <http://doi.org/10.1590/S0482-50042010000200002>.
5. Silva LFC, Oliveira EFC. Caracterização química e metalográfica dos aços inoxidáveis de implantes removidos de pacientes. *Acta Ortop Bras*. 2011;19(5):280-5. <http://doi.org/10.1590/S1413-78522011000500003>.
6. Asoh H, Nakatani M, Ono S. Fabrication of thick nanoporous oxide films on stainless steel via DC anodization and subsequent biofunctionalization. *Surf Coat Tech*. 2016;307:441-51. <http://doi.org/10.1016/j.surfcoat.2016.09.025>.
7. Le Guéhennec L, Soueidan A, Layrolle P, Amouriq Y. Surface treatments of titanium dental implants for rapid osseointegration. *Dent Mater*. 2007;23(7):844-54. <http://doi.org/10.1016/j.dental.2006.06.025>.
8. Mahapatro A. Bio-functional nano-coatings on metallic biomaterials. *Mater Sci Eng C*. 2015;55:227-51. <http://doi.org/10.1016/j.msec.2015.05.018>.
9. Kowalski D, Kim D, Schmuki P. TiO<sub>2</sub> nanotubes, nanochannels and mesopore: self-organized formation and applications. *Nano Today*. 2013;8(3):235-64. <http://doi.org/10.1016/j.nantod.2013.04.010>.
10. Variola F, Brunski J, Orsini G, Oliveira PT, Wazen R, Nanci A. Nanoscale surface modifications of medically-relevant metals: state-of-the-art and perspectives. *Nanoscale*. 2011;3(2):335-53. <http://doi.org/10.1039/C0NR00485E>.
11. Wang Y, Li G, Wang K, Chen X. Fabrication and formation mechanisms of ultra-thick porous anodic oxides film with controllable morphology on type-304 stainless steel. *Appl Surf Sci*. 2020;505:144497. <http://doi.org/10.1016/j.apsusc.2019.144497>.
12. Saha SK, Park YJ, Kim JW, Cho SO. Self-organized honeycomb-like nanoporous oxide layer for corrosion protection of type 304 stainless steel in an artificial seawater medium. *J Mol Liq*. 2019;296:111823. <http://doi.org/10.1016/j.molliq.2019.111823>.
13. Doff J, Archibong PE, Jones G, Koroleva EV, Skeldon P, Thompson GE. Formation and composition of nanoporous films on 316L stainless steel by pulsed polarization. *Electrochimica Acta*. 2011;56(9):3225-37. <http://doi.org/10.1016/j.electacta.2011.01.038>.
14. Burleigh TD, Schmuki P, Virtanen S. Properties of the Nanoporous anodic oxide electrochemically grown on steel in hot 50% NaOH. *J Electrochem Soc*. 2009;156(1):C45. <http://doi.org/10.1149/1.3021029>.
15. Burleigh TD, Dotson TC, Dotson KT, Gabay SJ, Sloan TB, Ferrell SG. Anodizing steel in KOH and NaOH solutions. *J Electrochem Soc*. 2007;154(10):C579. <http://doi.org/10.1149/1.2767417>.
16. Yilmaz B, Pazarceveren AE, Tezcaner A, Evis Z. Historical development of simulated body fluids used in biomedical applications: A review. *Microchem J*. 2020;155:104713. <http://doi.org/10.1016/j.microc.2020.104713>.
17. Callister JWD. *Ciência e engenharia de materiais uma introdução*. 7. ed. Rio de Janeiro: LTC; 2008.
18. Young L. *Anodic oxide films*. Talanta: Elsevier; 1961.
19. Marcus P, Maurice V. Passivity of metals and alloys. In: Caren RW, Haseb P, Kramer EJ, editors. *Materials science and technology*. Weinheim: Wiley-VCH Verlag GmbH & Co KGaA; 2000. p. 13-29.
20. Kirchheim R, Heine B, Fischmeister H, Hofmann S, Knotz H, Stolz U. The passivity of iron-chromium alloys. *Corrosion Science*. 1989;29(7):899-917.
21. Calinski C, Strehlow H. ISS depth profiles of the passive layer on Fe/Cr alloys. *J Electrochem Soc*. 1989;136(5):1328-31. <http://doi.org/10.1149/1.2096915>.
22. Klimas V, Pakštas V, Vrublevsky I, Chernyakova K, Jagminas A. Fabrication and characterization of anodic films onto the type-304 stainless steel in glycerol electrolyte. *J Phys Chem C*. 2013;117(40):20730-7. <http://doi.org/10.1021/jp407028u>.
23. Conrado R. Avaliação da resistência à corrosão de aços inoxidáveis coloridos por processos eletroquímicos [thesis]. São Carlos: Universidade Federal de São Carlos; 2003.
24. Mello LS. Estudo de corrosão localizada dos aços inoxidáveis em sistemas de resfriamento industrial [projeto de graduação]. Rio de Janeiro: Universidade Federal do Rio de Janeiro; 2011 [cited 2023 Aug 15]. Available from: <http://monografias.poli.ufrj.br/monografias/monopoli10003539.pdf>
25. Ansell RO, Dickinson T, Povey AF. An X-ray photo-electron spectroscopic study of the films on coloured stainless steel and coloured 'Nilomag' alloy 771. *Corros Sci*. 1978;18(3):245-56. [https://doi.org/10.1016/S0010-938X\(78\)80021-3](https://doi.org/10.1016/S0010-938X(78)80021-3).
26. Lin FH, Hsu YS, Lin SH, Sun JS. The effect of Ca/P concentration and temperature of simulated body fluid on the growth of hydroxyapatite coating on alkali-treated 316L stainless steel. *Biomaterials*. 2002;23(19):4029-38. [http://doi.org/10.1016/S0142-9612\(02\)00154-0](http://doi.org/10.1016/S0142-9612(02)00154-0).
27. Giordano EJ, Alonso-Falleiros N, Ferreira I, Balancin O. Electrochemical behavior of two austenitic stainless steel biomaterials. *Rev Esc Minas*. 2010 [cited 2023 Aug 15];6:159-66. <http://www.scielo.br/pdf/rem/v63n1/27.pdf>
28. Panda B, Sujata M, Madan M, Bhaumik SK. Stress corrosion cracking in 316L stainless steel bellows of a pressure safety valve. *Eng Fail Anal*. 2014;36:379-89. <http://doi.org/10.1016/j.engfailanal.2013.11.007>.
29. Gentil V. *Corrosão*. 6. ed. Rio de Janeiro: LTC; 2012.
30. El-Hadad S, Khalifa W, Nofal A. Surface modification of investment cast-316L implants: microstructure effects. *Mater Sci Eng C*. 2015;48:320-7. <http://doi.org/10.1016/j.msec.2014.12.038>.
31. Ziętała M, Durejko T, Polański M, Kunce I, Płociński T, Zieliński W, et al. The microstructure, mechanical properties and corrosion resistance of 316 L stainless steel fabricated using laser engineered net shaping. *Mater Sci Eng A*. 2016;677:1-10. <http://doi.org/10.1016/j.msea.2016.09.028>.
32. Bauer S, Schmuki P, von der Mark K, Park J. Engineering biocompatible implant surfaces: Part I: Materials and surfaces. *Prog Mater Sci*. 2013;58(3):261-326. <http://doi.org/10.1016/j.pmatsci.2012.09.001>.
33. Coelho PG, Jimbo R. Osseointegration of metallic devices: current trends based on implant hardware design. *Arch Biochem Biophys*. 2014;561:99-108. <http://doi.org/10.1016/j.abb.2014.06.033>.
34. Gonçalves MC, Santos BAF, Souza RC, Mendes E Jr, Simões TA, Oliveira JR, et al. Influência da concentração de cloreto de sódio na formação dos filmes de sulfeto de ferro e carbonato de ferro no aço API X65 em meios contendo CO<sub>2</sub> e H<sub>2</sub>S. *Intercorr*. 2018;1:21.
35. Brooks EK, Brooks RP, Ehrensberger MT. Effects of simulated inflammation on the corrosion of 316L stainless steel. *Mater Sci Eng C*. 2017;71:200-5. <http://doi.org/10.1016/j.msec.2016.10.012>.
36. Padilha AF, Guedes LC. Aços inoxidáveis austeníticos: microestrutura e propriedades. São Paulo: Hemus Editora; 1994.
37. Ribeiro DV, Souza CAC, Abrantes JCC. Uso da espectroscopia de impedância eletroquímica (EIE) para monitoramento da corrosão em concreto armado. *Rev IBRACON Estrut Mater*. 2015;8:529-49. <http://dx.doi.org/10.1590/S1983-41952015000400007>.
38. Calderon Velasco S, Lopez V, Almeida Alves CF, Cavaleiro A, Carvalho S. Structural and electrochemical characterization of Zr-C-N-Ag coatings deposited by DC dual magnetron sputtering. *Corros Sci*. 2014;80:229-36. <http://doi.org/10.1016/j.corsci.2013.11.036>.
39. Cao Z, Kong G, Che C, Wang Y. Influence of Nd addition on the corrosion behavior of Zn-5%Al alloy in 3.5wt.% NaCl solution. *Appl Surf Sci*. 2017;426:67-76. <http://doi.org/10.1016/j.apsusc.2017.07.109>.

40. Colpaert H. Metalografia dos produtos siderúrgicos comuns. 4. ed. São Paulo: Blucher; 2008.
41. Vicente AA, Cabral DA, Marques IJ, Santos TFA, Espinosa DCR, Tenório JAS. Caracterização microestrutural das camadas protetivas de óxidos formados nas superfícies de um aço inoxidável austenítico laminado (253 Ma®) oxidado a altas temperaturas ao ar. In: 72nd ABM Annual Congress; 2017; São Paulo. Proceedings. São Paulo: ABM; 2017. p. 54-65. <http://doi.org/10.5151/1516-392X-30090>.
42. Anderson JA, Lamichhane S, Mani G. Macrophage responses to 316L stainless steel and cobalt chromium alloys with different surface topographies. *J Biomed Mater Res A*. 2016;104(11):2658-72. <http://doi.org/10.1002/jbm.a.35808>.